INTEGRATION OF CORE, LOG, AND TEST DATA FOR SATURATION MODELING

E. F. deZabala and J. Gidman
Chevron Petroleum Technology Company

ABSTRACT

Integrated saturation modeling is a valuable product of the application and interpretation of available core, log, and test data. Integrated saturation models quantify uncertainty and improve estimates of OOIP and reserves. Saturation models add value for core/log analysts by: 1) focusing efforts on the most valuable applications and 2) adding new uses for previously unused or contradictory data. Two cases are presented.

In case A, new interpretations of old results are allied with modern core/log interpretation to improve OOIP and recovery estimates. OOIP estimates increased by 25%. Increased OOIP reduced anomalous recovery estimates, more than 80%, to a high but reasonable value of ~65%. High recovery is due to effective gravity drainage. Integrated saturation modeling results for the mature reservoir have proven the business value for improved special core analysis (SCAL) tests.

Case B illustrates saturation modeling in a heterogeneous, mixed lithology setting where different vintages of core, log, and test data are reconciled. Quantifying uncertainty in OOIP and recovery estimates from integrated saturation models was important for moving to the next phase of development. Significant uncertainties in S_{wi} and S_{orw} convinced the operating unit to core additional wells and to apply more sophisticated methods to narrow the band of uncertainty.

CASE A

Background. Field A is mature; with two main sands, H-03 and H-04, undergoing bottom water drive augmented by injection. More than 30 wells penetrate both sands. Upon review of all data, ultimate recoveries appeared to be too high, more than 80% OOIP. Such high recovery is possible for laboratory samples but is questionable for a reservoir. Log interpretation problems were suspected because many logs were recorded decades ago using unfocused resistivity logs. Logs did not yield consistent S_w. In wells #16, #17, and #18, sands are at similar height above free water, are in the same facies, and have equivalent shale content, suggesting that they should have similar S_w. That is not the case. Log analysis gave the following average values for the H-04 sand:

- Well #16 $\phi = 26\%$ $S_{wi} = 40\%$
- Well #17 $\phi = 28\%$ $S_{wi} = 20\%$
- Well #18 $\phi = 25\%$ $S_{wi} = 30\%$

In sand/shale sequences in a low-salinity environment, conventional resistivity analysis yields inconsistent S_{wi} values that are too large. An alternative analysis was needed.

Analysis Tools. A two-step core-log approach to estimating S_{wi} was devised. Core was available over the entire H-03/04 interval from the recently drilled well #37. A modern log suite was available in well #37.

The first approach uses SCAL tests to obtain measurements for S_{wi} and mineralogy, and builds a transform to S_{wi} from log-calculated V_{shale}. V_{shale} was chosen because: *1)* it is a robust parameter based on logs available in all wells, *2)* gamma ray response has better spatial resolution (~1.5 feet) than the induction resistivity logs (~5 feet or more) and *3)* V_{shale} is a measure of clay content

that is expected to correlate with S_{wi}. We term the approach CLAWS (Core-Log Analysis for Water Saturation).

The second approach uses petrophysically-based thin-bed modeling to calculate S_w in well #37. The forward modeling method uses log-based V_{shale} to formulate thinly-bedded sequences. Shale layers are assigned constant resistivity (R_{sh}=2.5 ohm-m) and S_w=1. Resistivity is calculated using Archie's formula $R_T = R_w \phi^{-m} S_w^{-n}$, with R_w=0.32 ohm-m, m=1.8 and n=1.9. All electrical parameters were determined from well #37 core analysis. The only unknown is S_w in sands. To solve for S_w, sands are populated with a series of constant S_w populations. For each constant S_w population, apparent resistivity is determined by solving the electromagnetic wave dispersion equation for the induction resistivity tool response. A first-pass S_w profile is obtained by matching calculated resistivity with the observed response at each depth. Final S_w is determined by iterative comparison of calculated and observed resistivity, using the first-pass S_w profile as input.

Note that both CLAWS and thin-bed resistivity modeling are required for field calculations. In recent wells, focused induction resistivity response can be corrected using thin-bed modeling. The simpler CLAWS algorithm is applicable to all wells, including older wells (pre-1983). Resistivity modeling is not possible with older tool responses.

Results. Figure 1 plots S_{wi} vs. V_{shale} for plugs from the H-03/04 reservoirs. S_{wi} was chosen to equal S_w at an oil/water capillary pressure (P_c) equal to 30 psia. V_{shale} is a log-derived parameter. We found the most appropriate V_{shale} to be the minimum of the Density and Steiber[9] V_{shale} parameters. Density V_{shale} is obtained by linear interpolation between "clean sand" and "shale" bulk density responses. Steiber[9] V_{shale} is determined by quadratic interpolation between "clean sand" and "shale" baselines of the gamma ray response. Transition zone effects were not considered as the intervals of interest are high above the WOC. Linear regression of S_{wi} vs. V_{shale} yields the following transform:

$$\mathbf{S_{wi}\,(\%) = 8.9(5.9) + 0.56(0.11)*V_{shale}\,(\%) \quad R^2 = 0.83.} \qquad \mathbf{(1)}$$

Numbers in parentheses are the standard errors for each parameter.

Parameter uncertainty is not due to experimental error alone. There are real differences in mineralogy. Analysis revealed that the best facies, channel sands, contain only kaolinite, while bar sands contain similar amounts of kaolinite and illite. Shales contain 3-4 times as much kaolinite as illite. The low gamma ray response of kaolinite relative to illite places a shale baseline at an inappropriate value for different sands: channel sands yield V_{shale} too low and bar sands yield V_{shale} too high. Uncertainty in S_{wi} at low V_{shale} reflects the abundance of fine particles (e.g. kaolinite and/or silt) relative to sand grains. With poorer sorting, we expect an increase in S_{wi} and a decrease in ϕ. To account for the rock differences noted above, we derived a bilinear transform of S_{wi} from V_{shale} and ϕ as:

$$\mathbf{Swi\,(\%) = 101.4(17.1) + 0.195(0.080)*Vshale - 3.48(0.64)*\phi \quad R^2 = 0.97.} \qquad \mathbf{(2)}$$

S_{wi}, V_{shale}, and ϕ are in %. Equation (2) yields a better fit to the available data and it follows expected trends, but it was not applied field-wide because it is based on only a few points.

In Table 1, we compare log-calculated S_w to CLAWS S_{wi} in 4 wells. For the older wells (#16-#18), CLAWS S_{wi} is more consistent as well as significantly lower than log-derived S_w.

Table 1: Comparison of Log- and CLAWS-derived Sw

Well	H-03 Sand		H-04 Sand	
	Log Swi	CLAWS Swi	Log Swi	CLAWS Swi
#16	23%	10%	40%	9%
#17	34%	19%	21%	10%
#18	35%	20%	30%	10%
#37	15%	12%	*waterflooded*	9%

The comparison builds confidence in the transform because log-derived S_w is close to CLAWS S_{wi} in the unswept H-03 sand of well #37, a modern well.

Dashed lines in Fig. 1 indicate uncertainty associated with the S_{wi}-V_{shale} transform derived from oil/water, porous plate P_c tests. Using the transform, most likely OOIP estimates increased by 25% (125 MM BBL). Parameter uncertainty indicates OOIP increases ranging from 90 to 140 MM BBL.

Results from companion mercury intrusion P_c tests yield a similar S_{wi}-V_{shale} transform. Mercury P_c was converted to "oil/water" P_c using simple default values for the ratio of interfacial forces (e.g., 370 dyne/cm and 30 dyne/cm). For reservoir A, mercury intrusion and oil/brine porous plate P_c tests yield similar results.

Figure 2 compares CLAWS-S_{wi} with S_w from thin-bed modeling for the H-03 sand. At the top of the H-03 sand, both S_w are close. Both are less than 10%. Deeper in the sand, log-derived S_w tends to be slightly larger than CLAWS S_{wi}. Part of that difference may reflect uncertainty in the transform at low V_{shale}. Some of the difference may be due to initial stages of waterflood displacement.

Figure 3 compares CLAWS S_{wi} with S_w from thin-bed modeling for the H-04 sand in Well #37. Note that the H-04 sand is thicker and contains more thinly-bedded shales than the H-03 sand. At the time of coring, most of the H-04 had been swept by water. The WOC is located at a depth of ~9045 feet. Above the WOC, CLAWS-S_{wi} is very close to log-derived S_w. Below the new WOC, log-derived S_w clearly show massive influx of water. Thinly bedded shalesare not continuous and appear to have only local effects on waterflood sweep.

Log-derived S_w's indicate S_{orw} as low as ~10% in the best intervals. Archie's Law, that relates S_w to resistivity, should have minimal error in higher conductivity, water-invaded sands. There is some concern that the saturation index, n, derived from drainage tests may not be the best to use for an imbibition process. However, additional data confirms low S_{orw}. Using the method reported by Rathmell et al.[1], we correct S_o from routine core analysis (e.g., PK&S) to yield S_{orw} estimates. The H-04 core easily meets all of Rathmell et al.'s criteria. The PK&S S_o were corrected using the oil formation volume factor (Bo=1.436 RB/STB). We do not use Rathmell et al.'s bleeding correction and do not use a compaction correction because core and log ϕ were almost exactly the same. Figure 3 compares corrected PK&S S_o with log-derived S_w. In the best sand intervals (e.g., 9050-9080 ft and 9105-9120 ft), both methods are in agreement, with S_{orw} in the range of 10% to 15%. For some thin sands bounded by shale, differences between log-derived S_o and S_{orw} indicate bypassed oil.

Two methods show that S_{orw} in the best sands falls in the range of 10% -15%. Available SCAL data indicate higher S_{orw}. Two conventional water/oil relative permeability tests on samples from the H-04 indicate S_{orw} of 26% and 29%, respectively. Single-point spontaneous imbibition tests

on 26 plugs (H-03) and 47 plugs (H-04) from well #9 indicate average S_{orw} of 24% and 23%, respectively for the H-03 and H-04 sands.

Why is there a large difference in measured and observed S_{orw}? Laboratory tests rely solely on the balance between viscous and capillary forces to establish S_{orw}: some oil may be bypassed by viscous fingering and tests are terminated after only a few pore volumes of injection. Also, samples may have been extracted to a strongly water-wet state that does not represent the reservoir. Spontaneous imbibition tests rely solely on capillary forces to establish S_{orw}, with the assumption of a strongly water-wet state. Both tests ignore the combined effects of gravity and wettability. To attain low S_{orw} (~10%), Hirasaki[2] demonstrated that several conditions are necessary: 1) mixed wettability, 2) large drainage times, 3) sand thickness large compared to the capillary transition zone, and 4) low mobility ratio (e.g., low oil viscosity) The H-03/04 reservoirs meet all criteria. Upward movement of the WOC ranged from ~5 to 7 feet/year. Mineral analyses indicate that kaolinite is a major clay mineral present in the H-03//04 sands. Kaolinite has been associated with mixed wet behavior in sandstones[3]. For Prudhoe Bay sandstones, Jerauld[4] found that mixed wet behavior was associated with low S_w (i.e., high in oil column), where quartz surfaces may become non-water-wet. In 1996, Kokkedee et al.[8] demonstrated that careful, modern SCAL tests support S_{orw} values 10 to 15 saturation units lower than older estimates for a worldwide sampling of Shell's reservoirs. For case A, field evidence indicates that Sorw is ~10 saturation units lower than laboratory results.

Case A Summary. A S_{wi}-V_{shale} transform for the H-03/04 sands was developed based on SCAL, log analysis, and mineralogy. S_{wi} from the transform are 15-20% lower than S_w calculated by conventional resistivity analysis. OOIP was increased by 25% (125 MM BBL). With the new OOIP, ultimate recovery is estimated to be ~65% rather than the initial estimate of about 80%.

Integrating core and log results provides compelling evidence for low S_{orw} (~10-15%) by gravity drainage. Efficient gravity drainage is associated with mixed wettability. This has prompted us to perform additional SCAL tests, namely centrifugal water/oil displacements and wettability tests, to account properly for gravity drainage effects in this and similar reservoirs in the region.

CASE B

Background. Field B is undeveloped with structure and stratigraphy defined by 6 wells. The oil-bearing Inca Formation consists of heterogeneous mixtures of clastics and carbonates with very few pure end members. The Inca is divided into three intervals: the Tabla, Lake, and Blue members as illustrated in the following table:

Interval	Lithology	Reservoir Potential
Blue 1	Bedded silt/shale	Intermediate reservoir
Blue 2	Bedded silt/shale,carbonate cement	Poor reservoir
Blue 3	Carbonate cemented argillaceous siltstone	Non-reservoir
Lake-1	Bedded silt/shale	Reservoir
Lake-2	Burrow mottled carbonate siltstone	Reservoir
Lake-3	Carbonate cemented argillaceous siltstone	Non-reservoir
Tabla-1 to Tabla-3 (upper Tabla)	Burrowed silty carbonate	Reservoir
Tabla-4 to Tabla-5 (lower Tabla)	Bedded silt/shale, carbonate cement	Reservoir

In the mid-1980's the first core was taken in well 35-2X. Development was suspended until recently, with four additional wells drilled and cored in 1997. Only the 47-3 core covers the complete stratigraphic section. In addition to core-log depth matching, a significant amount of work involved reconciling different types and vintages of wireline log responses, PK&S data, special core analyses, and drillstem tests into a coherent picture of reservoir quality. Conventional resistivity analysis was not appropriate in the thin-bedded, heterogeneous rocks. In trying to reconcile the available, we realized that significant uncertainty existed in any description. To quantify that uncertainty, we use integrated saturation modeling.

Analysis Tools. There are ~1500 feet of core from the Inca in Field B. Core coverage is summarized in Table 2.

Table 2: Available PK&S Data

Well	Cored Intervals	PK&S plugs (1")	Full diameter
35-2X	Blue-1 to Lake-3 and Tabla-1 to Tabla-3	252	none
35-3	Blue-1 to base Lake-3	353	none
46-9	Blue-1 to Tabla-1	313	none
47-3	Blue-1 to Tabla-5	611	24

PK&S consisted of ϕ, K_{air} , S_o and S_w from 1"-diam., horizontal plug samples with a sample spacing of ~1 foot. Full-diameter core analyses were conducted for bioturbated intervals of well 47-3, Tabla-1 and Lake-2, because 1" samples are too small to measure true permeability. In those zones, full-diameter measurements were performed on 24 samples. Subsequently, full-diameter samples were slabbed and sub-sampled into horizontal 1" diameter plugs. A transform was developed between permeabilities measured at both scales. The transform yielded the following result (K in md):

$$K_{Full\text{-}Diameter} = 30.672*(K_{PK\&S})^{0.4543}, \qquad (3)$$

SCAL results are available from wells 35-2X, 46-9, and 47-3, but test types are not consistent and coverage over several intervals is weak. Several types of P_c results are available. Single-point air/oil, drainage and imbibition P_c tests are available for a large number of plug samples from well 35-2X. More conventional, modern SCAL results are available for some of the recent cores. The different types of available SCAL results reflect the long delay in Field development and changes in methods. Table 3 summarizes available results by test type, interval, and well.

Table 3: Available Special Core Analysis Data

Well	Interval	Air/Oil Drainage & Imbibition P_c	Mercury P_c	Air/Brine P_c	Water/Oil Relative Permeability
35-2X	Blue	17	3	-	-
	Lake	60	19	-	-
	Tabla	28	17	5	6
46-9	Blue	-	2	-	-
	Lake	-	6	-	-
	Tabla	-	-	-	-
47-3	Blue	-	6	4	3
	Lake	-	2	3	4
	Tabla	-	2	1	1

Permeability Transform. A key part of saturation modeling is developing core-log permeability transforms that cover the range of data. For these heterogeneous rocks, it was difficult to develop

one transform that worked well for all rock types. Different relationships were tested and specific transforms were developed and written into a log-processing module. For all cases, the permeability being matched was the plug PK&S data. The more carbonate-rich lithologies (Lake-2 and Upper Tabla) are more appropriately measured by full-diameter analysis as shown by comparison of the plug and full-diameter data for well 47-3 and as shown in previous work (Gidman and Fischer[7]).

Permeability predicted from the transforms is compared to DST results over the same intervals in Table 4. Only a few usable DST results were available.

Table 4: Comparison of DST Permeability with Transform Permeability

Well	Interval	Average K (md) DST	Average K (md) transform
47-3	Lake-1	240 to *500?*	106
47-3	Lake-2	62	69
46-9	Lake-2	37	32
47-3	Mesa-1	1466.	210.

Agreement between DST results and the transform gave us confidence that the transform provides a suitable base case (Most Likely) for predicting permeability. However, the transform significantly under-predicts DST permeability for the burrowed/ bioturbated intervals: Lake-1 and Mesa-1 in Well 47-3. We surmise that 1" plugs are too small to capture the true permeability. Thus, two adjustments constitute the High-End case for permeability. First, we scale up permeability in the appropriate zones by applying Equation (3) to the base case. Second, although there is uncertainty regarding the tested interval in the Lake-1 in well 47-3, the transform under-predicts average DST permeability by a factor ranging from 2.5 to 5. To match the low end of the range, the transform is multiplied by a constant factor of 2.67. For the Low-End case, the base case transform is retained while different P_c parameters are used to predict S_w.

Capillary Pressure Model. Inca intervals exhibit low- to moderate permeability and are close to a known WOC. Transition zone effects are significant. Also, with the mixed clastic/carbonate setting and significant heterogeneity, a simple S_{wi}-V_{shale} transform is not applicable. To model S_w, we use a modified Brooks-Corey equation written as:

$$\mathbf{P_c = P_e*(S_w*)^{-1/\lambda} \quad . \qquad (4)}$$

P_e is the entry pressure (psia), λ is the dimensionless Brooks-Corey pore size distribution parameter, and S_w* is a normalized water saturation given by:

$$\mathbf{S_w* = (S_w - S_{wirr})/(1 - S_{wirr}) \quad . \qquad (5)}$$

S_{wirr} is "irreducible" water saturation. With known WOC in each zone, P_c is calculated as:

$$\mathbf{P_c(Z) = \Delta\rho_{ow}*g*(Z_{FWL} - Z)\ , \qquad (6)}$$

Z is depth at any given point, Z_{FWL} is the depth of the free water level (i.e., P_c=0) and $\Delta\rho_{ow}$*g is the known oil-water gradient (0.105 psia/foot). Eqs. (4), (5), and (6) can be re-written as:

$$\mathbf{S_w = S_{wirr} + (1 - S_{wirr})*\{P_c(Z)/P_e\}^{-\lambda} \quad . \qquad (7)}$$

Once P_e, λ, and S_{wirr} are known, S_w can be calculated at any point in the reservoir.

All P_c data were converted into equivalent oil/brine P_c curves using standard assumptions regarding interfacial tension and contact angle. For Hg P_c tests, we use only the low-pressure (P_{Hg}

≤ 3500 psia or oil/water $P_c \leq 30$ psia) data to determine parameters. Subsequently, P_e, λ, and S_{wirr} from Eqs. (4) and (5) were determined by best fit to a log-log plot of P_c versus S_w^*. To tie the model together, we look for trends in P_e, λ, and S_{wirr} versus permeability and/or stratigraphic interval.

Figure 4 plots P_e versus permeability. For samples from the Blue and Lake intervals, we find a power law relationship, $P_e = 9.037 * K_a^{-0.477}$. For the mostly upper Tabla intervals (Tabla-1 to 3), we find a slightly different relationship, $P_e = 6.674 * K_a^{-0.557}$. Lower entry pressures in the upper Tabla correspond to larger pores in the dolomitic packstone/ grainstone.

Figure 5 plots S_{wirr} versus permeability. There is significant scatter. Some of the scatter is due to differences in rock fabric (e.g., microporosity) in small plug samples. For similar samples, S_{wirr} from air/brine and mercury P_c tests are close. S_{wirr} from oil/water relative permeability tests are much higher than S_{wirr} from air/brine P_c tests using companion samples. Initially, the difference seemed puzzling; an oil/water system should represent reservoir conditions better. Review of the oil/water relative permeability results indicated that the heterogeneous samples were drained to S_{wirr} with low viscosity oil. Drainage tests were not conducted in the proper flow regime to overcome end effects. Some mobile water is bypassed due to viscous fingering. Some is retained due to end effects. Relative permeability tests exhibited early water breakthrough, suggesting the presence of mobile water. S_{wirr} from the oil/water tests are not reliable. S_{wirr} from the P_c tests, which are not affected by artifacts, best represent the reservoir. A best linear fit of S_{wirr} to $\log_{10}(K)$ yields $S_{wirr} = 0.4143 - 0.1006 * \log_{10}(K)$. That relationship is used for the base case (Most Likely) and the High-End case. For the Low-End case, the linear relationship is adjusted using the standard errors in each parameter to yield: $S_{wirr} = 0.4628 - 0.0870 * \log_{10}(K)$.

Pore-size distribution parameter, λ, did not exhibit a trend with permeability. By interval, average λ values are summarized in Table 5. Lower values of λ indicate wider pore size distributions.

Table 5: Brooks-Corey λ parameters by interval

Interval	Average λ
Blue-1 to Blue-3	0.69
Lake-1	1
Lake-2 and Lake-3	0.85
Tabla-1 to Tabla-3 (upper Tabla)	0.81
Tabla-4 to Tabla-5 (lower Tabla)	~1

A large number (105) of single-point air/oil drainage and imbibition P_c tests are available from well 35-2X. Plug samples from Blue (17), Lake (60), and Tabla (28) intervals were saturated with oil and drained to constant oil saturation (S_{oi}) with air (P_c=15 psia). Each sample was allowed to spontaneously imbibe oil until constant trapped gas saturation (S_{gt}) was attained. According to Land[6], the air/oil fluid system is a good analogue for oil/ water in a strongly water-wet rock. S_{oi} and S_{gt} from an air/oil system can be mapped to S_{wi} and S_{orw} from an oil/water system. The single-point tests were not conducted at a high enough P_c to attain S_w close to S_{wirr}. But the relationship between initial and final non-wetting phase saturations reveals information about the pore structure. Land[6] defined a trapping constant as:

$$\text{“C”} = 1/S_{orw} - 1/S_{oi} . \qquad (8)$$

For rocks with similar pore structure, “C” should be constant. Land[6] found “C” ranging from ~2 to 5. Lower values of “C” indicate more trapping for the same initial oil saturation (i.e., wider pore size distribution).

Figure 6 plots "C" versus permeability for the air/oil tests from well 35-2X. Different intervals appear to exhibit nearly constant "C" values. The upper Tabla, which has wider pore-size distribution, yields an average "C" = 1.25. Six water/oil relative permeability tests, conducted using plug samples from the upper Tabla of well 35-2X, yield an average "C" = 1.26. For the Lake intervals, average "C" = 2.37, which reflects a narrower pore size distribution. Water/oil relative permeability tests on Lake samples from well 47-3 indicate similar "C" values. Water/oil relative permeability tests on Blue samples from well 47-3 suggest an average "C" = 3.44. "C" values are listed in Table 6.

Table 6: Land's Trapping Constants

Interval	"C" Low End Case -P90	Base Case "C" Most Likely Case-P50	"C" High End Case-P10
Blue	2.94	3.44 (0.50)	3.94
Lake	1.90	2.37 (0.47)	2.84
Tabla-1 to Tabla-3	0.86	1.25 (0.39)	1.64
Table-4 to Tabla-5	1.85	2.30 (0.45)	2.75

Numbers in parentheses are standard deviations. Base case "C" corresponds to the average values; Low-End and High-End "C" values are adjusted by the standard deviation.

Results. S_{wi} profiles are predicted using Eqs. (4)–(7). P_e and S_{wirr} are functions of permeability using the core-log transform as input. λ is constant for each zone. P_C is calculated as a function of height above the FWL. Tabla and Lake share the same WOC at -1990 feet TVDSS, while the WOC for the Blue interval occurs at –1870 feet TVDSS. During initial calculations, S_{wi} profiles for well 47-3 did not match the first occurrence of oil. Close examination of core photographs revealed oil at a depth of –2024 feet TVDSS, close to the bottom of the cored interval. Placing a new FWL at –2026 feet TVDSS yielded a base case S_{wi} that matched the first occurrence of oil as well as the shape of the transition zone.

Figure 7 plots transform and core permeability and S_w versus depth in Well 46-9. Three plotted S_w profiles correspond to: High-End, Most Likely, and Low-End cases . Overall there is acceptable correspondence between transform and measured permeability. The WOC occurs at 2090 ft (measured depth). This corresponds to tight rocks in the Lake-3, hence there appears to be a longer than expected transition zone. Predicted S_w shows a reasonable match to core data.

Using Land's trapping constants for each interval, waterflood S_{orw} is estimated from S_{oi}. Thus both S_{wi} and waterflood movable oil saturation (S_{oi}–S_{orw}) can be estimated as a function of depth. Table 7 summarizes average ϕ, average and median permeability, and S_{wi} and movable oil saturations for each well on a zone-by-zone basis. Figure 8 plots average S_{wi} and movable oil saturation versus average permeability for each well penetration into one of the most important reservoir intervals in Field B: Lake-1. The points represent the Most Likely case and the lines indicate the uncertainty range from the Low-End to the High-End results. The range of uncertainty is large enough to warrant additional SCAL testing for future cored wells.

Case B Summary. Case B represents a first trial of saturation modeling in a complex, heterogeneous, mixed carbonate/siliciclastic setting. Log responses of different vintages were integrated with DST results, and routine and special core analyses to yield a saturation model that quantifies significant uncertainties in the available data.

Much of the core analysis data incorporated into the model were rudimentary. Significant uncertainties in S_{wi} and S_{orw} have convinced the operating business unit to core additional wells and to apply more sophisticated SCAL methods to narrow the band of uncertainty.

Table 7: Results of Saturation Modeling for Field B

Well	Interval	Thickness H (ft)	ϕ (Avg)	P50 Permeability K (Avg) md	P50 Permeability K(Median) md	INITIAL WATER SATURATION P90	INITIAL WATER SATURATION P50	INITIAL WATER SATURATION P10	MOVABLE OIL SATURATION P90	MOVABLE OIL SATURATION P50	MOVABLE OIL SATURATION P10
35-2X	**Blue-1**	**45**	**0.315**	**83**	**37**	0.541	**0.463**	0.463	0.274	**0.356**	0.372
35-3	**Blue-1**	**46**	**0.287**	**32**	**26**	0.620	**0.541**	0.541	0.208	**0.287**	0.301
46-9	**Blue-1**	**43**	**0.321**	**103**	**68**	0.503	**0.422**	0.422	0.302	**0.389**	0.406
47-2X	**Blue-1**	**22**	**0.314**	**101**	**66**	0.463	**0.389**	0.389	above GOC		
47-3	**Blue-1**	**52**	**0.347**	**131**	**73**	0.382	**0.302**	0.302	above GOC		
47-5	**Blue-1**	**44**	**0.326**	**113**	**58**	0.533	**0.452**	0.452	0.280	**0.367**	0.382
35-2X	**Blue-2**	**32**	**0.291**	**87**	**72**	0.459	**0.372**	0.372	0.333	**0.429**	0.447
35-3	**Blue-2**	**33**	**0.269**	**49**	**45**	0.605	**0.514**	0.514	0.214	**0.306**	0.321
46-9	**Blue-2**	**30**	**0.300**	**111**	**112**	0.446	**0.358**	0.358	0.344	**0.442**	0.461
47-2X	**Blue-2**	**25**	**0.293**	**145**	**144**	0.353	**0.269**	0.269	above GOC		
47-3	**Blue-2**	**29**	**0.317**	**123**	**118**	0.360	**0.278**	0.278	above GOC		
47-5	**Blue-2**	**31**	**0.306**	**122**	**98**	0.483	**0.391**	0.391	0.312	**0.413**	0.431
47-2X	**Blue-3**	**35**	**0.328**	**1.2**	**1.2**	0.731	**0.674**	0.674	above GOC		
47-3	**Blue-3**	**41**	**0.322**	**15**	**1.7**	0.623	**0.562**	0.562	above GOC		
47-3	**Blue-3**	**41**	**0.322**	**15**	**1.7**	0.623	**0.562**	0.562	above GOC		
35-2X	**Lake-1**	**94**	**0.256**	**36**	**32**	0.441	**0.362**	0.290	0.293	**0.388**	0.476
35-3	**Lake-1**	**99**	**0.234**	**17**	**12**	0.575	**0.496**	0.401	0.204	**0.287**	0.385
46-9	**Lake-1**	**90**	**0.264**	**46**	**36**	0.407	**0.327**	0.261	0.315	**0.415**	0.501
47-2X	**Lake-1**	**105**	**0.285**	**83**	**57**	0.342	**0.264**	0.211	0.366	**0.468**	0.546
47-3	**Lake-1**	**109**	**0.311**	**89**	**67**	0.329	**0.251**	0.201	0.378	**0.480**	0.555
47-5	**Lake-1**	**100**	**0.286**	**73**	**53**	0.403	**0.318**	0.249	0.318	**0.422**	0.512
35-2X	**Lake-2**	**86**	**0.209**	**18**	**16**	0.607	**0.518**	0.325	0.171	**0.259**	0.443
46-9	**Lake-2**	**79**	**0.215**	**28**	**24**	0.558	**0.470**	0.305	0.206	**0.298**	0.461
47-2X	**Lake-2**	**106**	**0.262**	**82**	**52**	0.377	**0.295**	0.224	0.338	**0.441**	0.534
47-3	**Lake-2**	**103**	**0.261**	**70**	**52**	0.366	**0.287**	0.216	0.350	**0.448**	0.541
47-2X	**Lake-3**	**40**	**0.272**	**5**	**4**	0.638	**0.563**	0.525	0.149	**0.223**	0.273
47-3	**Lake-3**	**47**	**0.296**	**26**	**12**	0.457	**0.383**	0.357	0.278	**0.367**	0.416
47-2X	**Tabla-1**	**24**	**0.195**	**29**	**24**	0.560	**0.412**	0.271	0.124	**0.251**	0.397
47-3	**Tabla-1**	**30**	**0.221**	**361**	**93**	0.324	**0.218**	0.180	0.250	**0.388**	0.471
47-2X	**Tabla-2**	**20**	**0.215**	**38**	**31**	0.586	**0.419**	0.281	0.110	**0.245**	0.389
47-3	**Tabla-2**	**24**	**0.209**	**162**	**98**	0.355	**0.247**	0.199	0.231	**0.366**	0.455
47-2X	**Tabla-3**	**23**	**0.144**	**27**	**22**	0.854	**0.632**	0.360	0.028	**0.128**	0.333
47-3	**Tabla-3**	**35**	**0.226**	**136**	**70**	0.371	**0.259**	0.205	0.221	**0.357**	0.450
47-3	**Tabla-4**	**49**	**0.284**	**67**	**42**	0.430	**0.312**	0.312	0.295	**0.423**	0.451

PRACTICAL APPLICATION OF SATURATION MODELING

For both cases, geo-cellular models were built using structural surfaces, internal markers and well data. For Field A, interpolation of V_{shale} traces at wells was used to produce a V_{shale} cube and cell properties were calculated for each cell based upon V_{shale} relationships. History match was straightforward, which lends credibility to the integrity of the model.

For Field B, three models were built; High-End, Low-End and Most Likely cases. Porosity and permeability interpolations were made from the porosity and (transform) permeability logs. Saturations were calculated (as described here) and production forecasts have been used in formulation of the development plan.

CONCLUSIONS

1. Integrated saturation modeling can be applied to new or mature fields in different geological settings.
2. Integrated saturation modeling often proves the business value associated with good core analysis results.
3. For new fields, quantifying uncertainty with saturation models helps identify the best applications for future core analysis.

REFERENCES

1. Rathmell, J.J. Braun, P.H., and Perkins, T.J.: "Reservoir Waterflood Residual Oil Saturation from Laboratory Tests," JPT (February 1973) pp. 175-185.
2. Hirasaki, G.J.: "Dependence of Waterflood Remaining Oil Saturation on Relative Permeability, Capillary Pressure, and Reservoir Parameters in Mixed Wet, Turbidite Sands," SPE Paper 30763, presented at the 1995 SPE Annual Technical Conference & Exhibition, Dallas, TX, U.S.A., 22-25 October, 1995.
3. Robin, M., Rosenberg, E. and Fassi-Fihri, O.: "Wettability Studies at the Pore Level: A New Approach by Use of Cryo-SEM," SPE Paper 22596, presented at the 1991 SPE Annual Technical Conference & Exhibition, Dallas, TX, U.S.A., 6-9 October, 1991, also **SPEFE** (March 1995).
4. Jerauld, G.R.: "General Three-Phase Relative Permeability Model for Prudhoe Bay, SPE Paper 36178 presented at the 7th International Petroleum Conference & Exhibition, Abu Dhabi, U.A.E., 13-16 October, 1996.
5. Corey, A.T.: *Mechanics of Heterogeneous Fluid in Porous Media*, Water Resources Publications – Fort Collins, CO, 1977, pp. 45-47.
6. Land, C.S.: "Comparison of Calculated with Experimental Imbibition Relative Permeability," SPE Paper 3360, presented at the 1971 SPE Rocky Mountain Regional Meeting, Billings, Montana, June 2-4, 1971.
7. Gidman, J., Conner, F.J., and Fischer, D.J.: "Deciphering Core and Log Porosity Differences and Evaluating the Scale Dependence of Core Analyses in a Complex Lithology." Proceedings of the Society of Core Analysts (1994) paper 9411 pp. 121-130.
8. Kokkedee, J.A., Boom, W., Frens, A.M., and Maas, J.G.: "Improved Special Core Analysis: Scope for a reduced residual oil saturation," SCA Paper 9601, presented at the 1996 SCA Conference, Montepellier, France, 8-10 September, 1996.
9. Steiber, S.J: "Pulsed Neutron Capture Log Evaluation – Louisiana Gulf Coast," SPE Paper #2961 presented at the 45th Annual Fall Meeting of the SPE of AIME, Houston, TX, October 4-7, 1970.

NOMENCLATURE

K	Permeability, md
P_c	Capillary pressure, psia
P_e	Entry pressure, psia
R_T	Measured resistivity, ohm-m
R_w	Water resistivity, ohm-m
S_{orw}	Waterflood residual oil saturation, % or fraction
S_w	Water saturation, % or fraction
S_{wi}	Initial water saturation, % or fraction
S_{wirr}	"Irreducible" water saturation, % or fraction
V_{shale}	Volume of shale calculated from wireline responses, %
Z	Depth, feet
$\Delta\rho_{ow}$	Oil-water density difference
λ	Brooks-Corey pore-size distribution parameter, dimensionless
ϕ	Porosity, % or fraction
CLAWS	Core-Log Analysis for Water Saturation
DST	Drillstem Test
FWL	Free water level ($P_c = 0$)
OOIP	Original oil in place
PK&S	Porosity, permeability and fluid saturations
SCAL	Special Core Analysis (Laboratory)
WOC	Water-oil contact

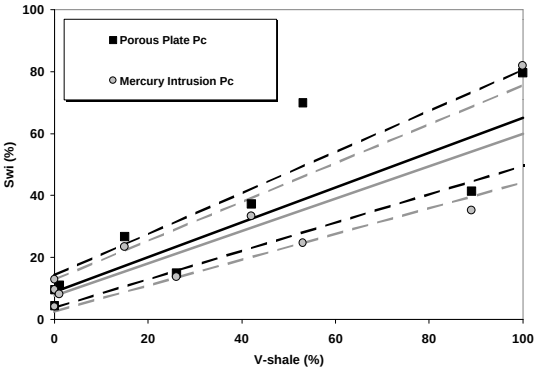

Figure 1: S_{wi} vs. V_{shale} from oil/water capillary pressure tests, Case A. Solid line is best-fit linear regression. Dashed lines indicate uncertainty level.

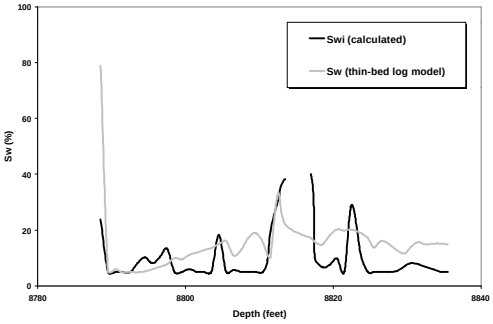

Figure 2: Transform-derived S_{wi} and corrected S_w from resistivity logs, H-H-03 sand, well #37, Case A.

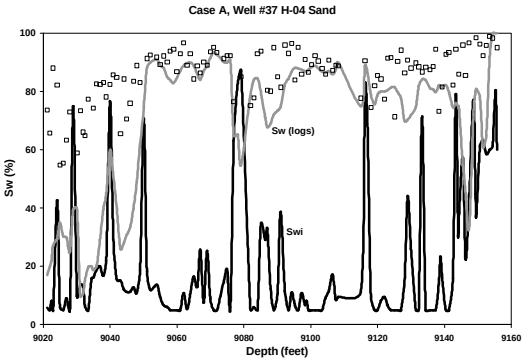

Figure 3: Transform-derived S_{wi} and corrected S_w from resistivity logs, H-04 sand, well #37, Case A.

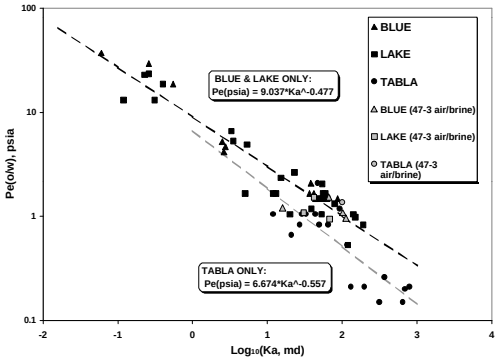

Figure 4: Oil/water entry pressure estimated from capillary pressure test results.

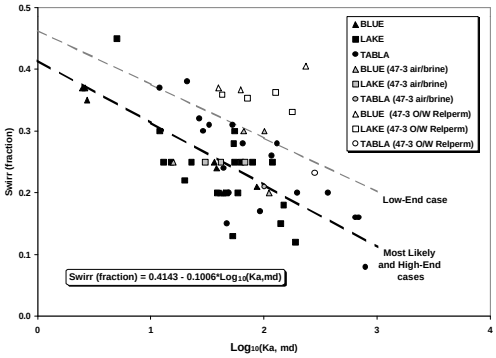

Figure 5: S_{wirr} vs. permeability, estimated from capillary pressure test results.

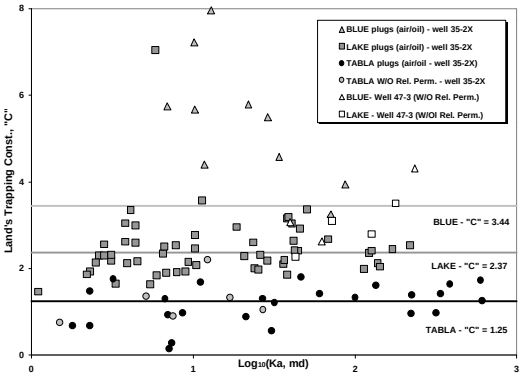

Figure 6: Land's trapping constants vs. permeability.

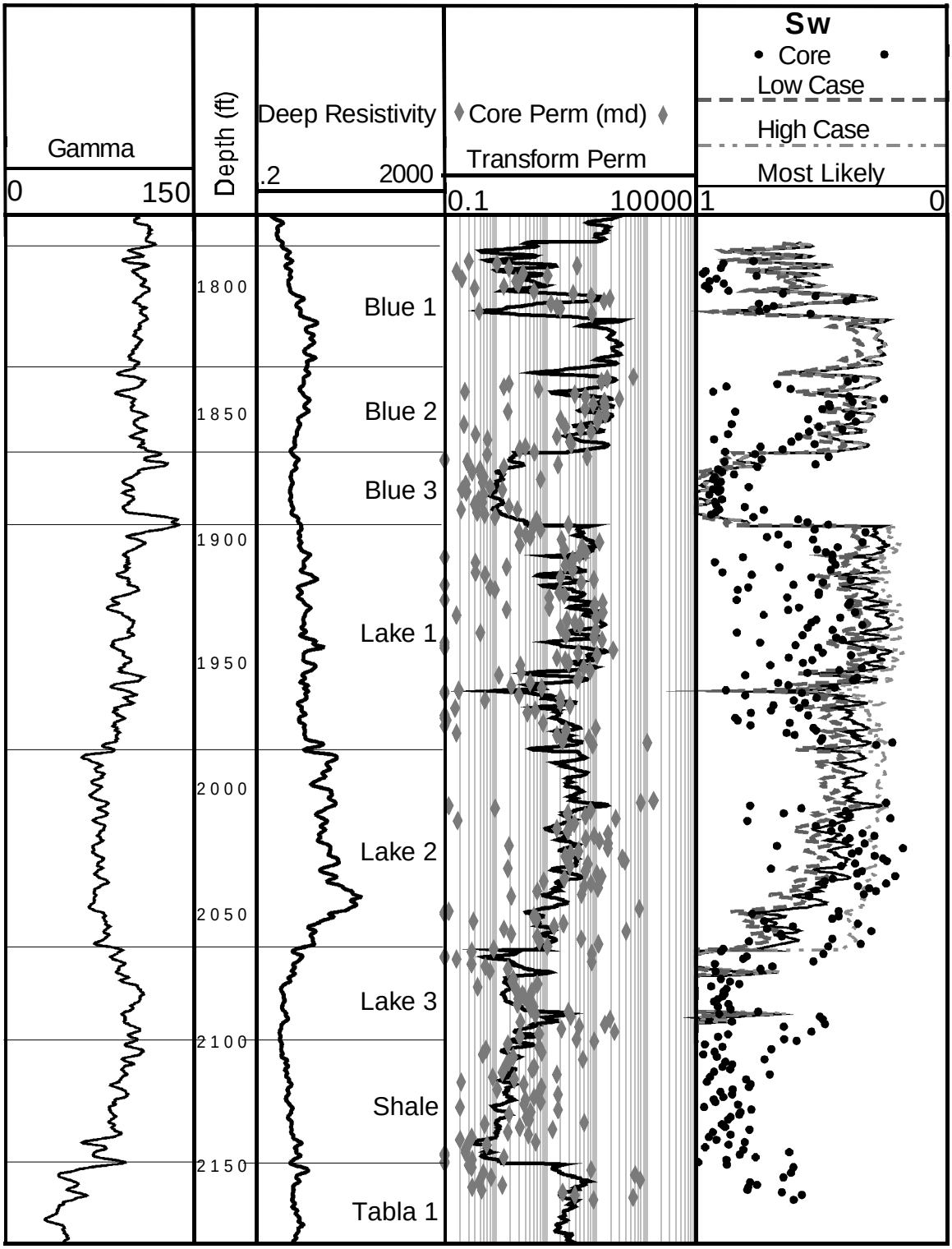

Figure 7. Wireline log responses, core data, predicted permeability and predicted S_{wi} for well47-3.

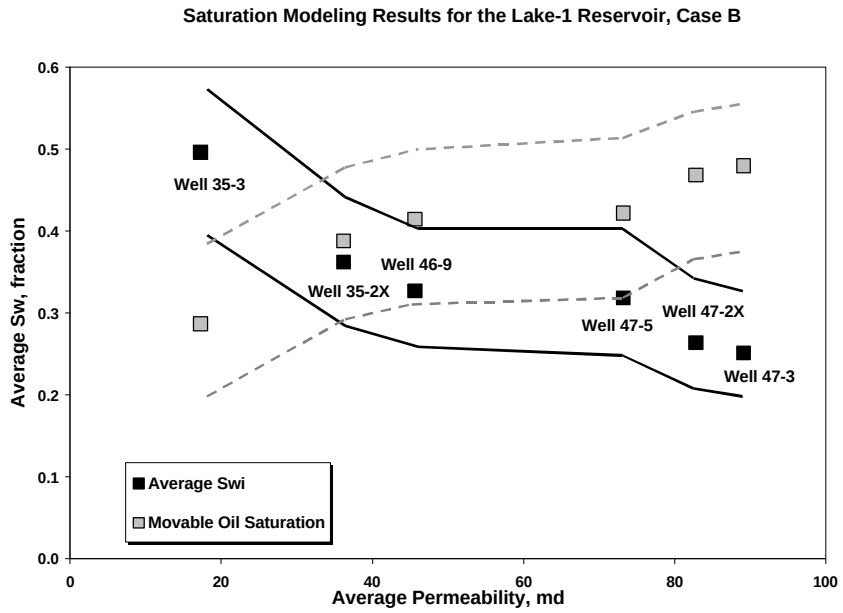

Figure 8: Saturation modeling results
for Lake-1 reservoir by well